Journal of the Mechanics and Physics of Solids 60 (2012) 1561–1581

Contents lists available at SciVerse ScienceDirect

Journal of the Mechanics and Physics of Solids

journal homepage: www.elsevier.com/locate/jmps

Generating virtual textile composite specimens using statistical data from micro-computed tomography: 3D tow representations

Renaud G. Rinaldi [a], Matthew Blacklock [a], Hrishikesh Bale [b], Matthew R. Begley [a], Brian N. Cox [c,*]

[a] University of California, Santa Barbara, CA 93106, USA
[b] University of California, Berkeley, CA 94720, USA
[c] Teledyne Scientific Co LLC, 1049 Camino Dos Rios, Thousand Oaks, CA 91360, USA

ARTICLE INFO

Article history:
Received 27 December 2011
Received in revised form
2 February 2012
Accepted 19 February 2012
Available online 27 February 2012

Keywords:
Textile composite
Stochastic microstructure
Virtual specimen
Topology
Geometry

ABSTRACT

Recent work presented a Monte Carlo algorithm based on Markov Chain operators for generating replicas of textile composite specimens that possess the same statistical characteristics as specimens imaged using high resolution x-ray computed tomography. That work represented the textile reinforcement by one-dimensional tow loci in three-dimensional space, suitable for use in the Binary Model of textile composites. Here analogous algorithms are used to generate solid, three-dimensional (3D) tow representations, to provide geometrical models for more detailed failure analyses. The algorithms for generating 3D models are divided into those that refer to the topology of the textile and those that deal with its geometry. The topological rules carry all the information that distinguishes textiles with different interlacing patterns (weaves, braids, etc.) and provide instructions for resolving interpenetrations or ordering errors among tows. They also simplify writing a single computer program that can accept input data for generic textile cases. The geometrical rules adjust the shape and smoothness of the generated virtual specimens to match data from imaged specimens. The virtual specimen generator is illustrated using data for an angle interlock weave, a common 3D textile architecture.

1. Introduction

This paper is part of a series devoted to establishing virtual tests for integral textile ceramic composites, which are a relatively new class of materials designed for use in hot structures (Marshall and Cox, 2008). Generally speaking, textile composites are a particular type of composite reinforced by continuous fibers, in which the fibers are first grouped into bundles (tows), which are then interlaced with one another, e.g., by weaving or braiding, in a great variety of possible ways (e.g., (Ko, 1989)). The resulting composite structures are heterogeneous and highly anisotropic in elasticity, strength, and transport properties on the scale of the tows, with many engineering properties intimately dependent on the continuity of fibers along tows and the discontinuity of material properties at tow boundaries. Critically, the topology of the tow interlacing determines patterns of stress and heat or electrical transport through the structure and is therefore a key factor distinguishing the capabilities of textiles from those of other composites or alloys. The presence of these key characteristics, i.e., the continuity of tows and their interlacing topology, logically dictates the formulation of reconstruction algorithms for replicating their

* Corresponding author.
E-mail address: bcox@teledyne.com (B.N. Cox).

0022-5096/$ - see front matter © 2012 Elsevier Ltd. All rights reserved.
doi:10.1016/j.jmps.2012.02.008

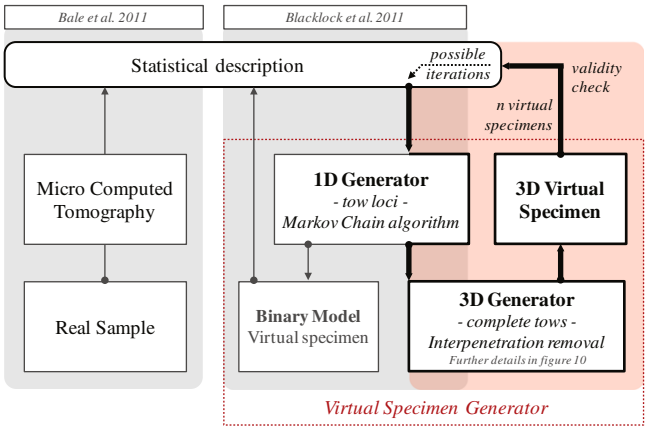

Fig. 1. Overall scheme for generating virtual specimens. Data from a real sample establish target statistics.

stochastic nature that are dissimilar to those developed for other material types (e.g., (Groeber et al., 2008; Jiao et al., 2009) and references therein).

The problem studied here is the formulation of an algorithmic generator for creating virtual specimens with a given textile architecture for use in simulations of thermomechanical performance and damage evolution. Like the real material, the virtual specimens feature stochastic microstructures. The virtual specimen generator assures that the most important statistics of the microstructure are close in value to those measured experimentally.

The new material presented in this paper fits into a larger overall scheme that combines acquisition and analysis of experimental data (Bale et al., 2011), calibration of generators against the data, generation of two classes of virtual specimens, one with 1D tow representations and the other with 3D tow representations, and validation of the achievement of target statistics in ensembles of virtual specimens (Fig. 1). The generation of 1D tow loci using a novel Markov chain algorithm has been described in Blacklock et al. (2012). The augmentations presented here use the same algorithm to generate trial 3D tow representations, which are converted into physically valid virtual specimens by the removal of interpenetrations and non-physical irregularities in shape resulting from numerical procedures. The present scheme has similar purpose to others proposed for virtual test simulations of textile composites (e.g., (Lomov et al., 2007)) or of other composite or alloy materials (e.g., (Cox and Yang, 2006; Pollock et al., 2008) and an early example relating random fatigue crack growth to microstructural variance in alloys (Cox, 1989)), but is distinguished by, among other things, addressing statistical variance.

As reported in the first paper in this series (Bale et al., 2011), geometrical data at the tow scale were recently acquired for one ceramic textile composite using synchrotron-based micron-resolution computed tomography (μCT). The material studied was a carbon fiber preform with an angle interlock architecture, which had been rigidified to constrain the geometry prior to imaging by depositing a coating of ceramic matrix on the tow (fiber bundle) surfaces. The raw μCT images were analyzed to identify the loci of the axes of all tows, along with variations in the shape and orientation of their cross-sections throughout the volume covered by the image. These data will be used here to calibrate the virtual specimen generator and test whether it has created statistically faithful replicas of the imaged specimens.

In a second paper in this series (Blacklock et al., 2012), a generator was developed that created virtual specimens in which each tow was represented by a 1D locus in 3D space. The complete set of interlacing tow loci are the required input for Binary Model simulations of textile composite performance (Cox et al., 1994; Xu et al., 1995; Yang and Cox, 2010). The geometry generator for 1D tow representations used a new formulation to calibrate a Markov Chain operator (Doob, 1953; Howard and Markov, 1971; Grinstead and Snell, 1997) to generate fluctuations in the coordinates of any tow axis by marching systematically along the tow's length.

The Markov Chain formulation is physically appropriate to the textile reconstruction problem, provided the dominant correlations are those along a tow, with correlations between tows being relatively weak. In fact, inter-tow correlations are not always weak; if they are not, the most general cases can be much more complicated to treat. For one relatively simple case, in which data imply a causal hierarchy among deviations on different tows, the Markov chain method can still be made to work with a simple variation and successfully replicates the experimentally measured correlations (Blacklock et al., 2012).

The Markov Chain formulation also requires the presence of the Markovian property, that a deviation at any point in the chain (position along a tow) depends only on the deviation of the previous point. This property appears to hold for physically significant deviations in the data set used in Blacklock et al. (2012).

In the present paper, the Markov Chain method of Blacklock et al. (2012) is augmented to include the characteristics of a tow that define its 3D shape, namely, the area, aspect ratio, and orientation of sequential cross-sections of the tow. The augmented Markov Chain algorithm is applied in combination with topological rules to remove interpenetrations or other ordering errors that inevitably occur when stochastic 3D bodies are generated by the Monte Carlo method. The correction

of ordering errors was unnecessary in the generator that created only 1D tow representations, because ordering errors virtually never occurred in that study (Blacklock et al., 2012). The centroids of different tows are separated by distances that are much larger than the deviations of any tow's centroid, so that 1D tow loci, which track the centroids, remain correctly ordered even in the stochastic structure. When generating 3D tow shapes, in contrast, tow boundaries are necessarily close to one another and random deviations commonly cause interpenetrations after intermediate steps in the generator algorithm, and occasionally cause part of one tow to appear completely on the wrong side of another tow. Topological rules correct such errors without ambiguity, since they embody the essential patterning that defines any single textile architecture. Topological algebras have a long history in textile science and have recently become a key part of generating textile models (Miyazaki et al., 1995; Grishanov et al., 2009a, 2009b; Xiao and Geng, 2010; Lomov et al., 2011). In the present work, simple and universally applicable topological ordering rules are proposed and procedures developed for their implementation within a probabilistic tow architecture generator.

A number of methods for generating solid models of textile reinforcement have been presented over the last several decades. The simplest of these assume simple shapes for individual tows, e.g., tow surfaces consisting of a combination of flat segments where two tows contact one another, and curved segments elsewhere. The most advanced of such methods approximately match the assumed shapes to sectional images of tows, but without analyzing stochastic deviations (Hivet and Boisse, 2005, 2008). Other researchers have sought to generate tow shapes close to those in experimental specimens via simulations of the mechanics of tow and preform deformation (Pastore et al., 1993; Wang and Sun, 2001; Lomov and Verpoest, 2002; Terpant et al., 2002; Badel et al., 2008; Miao et al., 2008; Sullivan and Yurus, 2010; Lomov et al., 2011). Mechanical models of textile deformation can in principle relate the details of the tow geometry in a textile to its processing history and are therefore a key part of an ultimate understanding of the whole cycle of textile design, manufacture, and performance. However, two major difficulties persist with deformation models: the mechanical history of a preform, including the loading conditions on tows and the kinetics of the weaving or braiding process, is often not well chronicled; and the constitutive laws for the dry fiber bundles (tows) in a preform are highly nonlinear and difficult to measure (Rugg and Cox, 2004). Thus the boundary conditions of a deformation simulation and the properties that should be assigned to the deforming material are not well known; the predictions are accordingly imperfect.

The question of how to remove interpenetrations between tows when generating textile models with realistic tow shapes is a longstanding challenge (Lomov et al., 2007). Those prior methods that have achieved greatest realism used mechanics-based algorithms, combining deformation simulations with methods of tracking the contact surfaces between tows. The difficult nonlinear problem of tracking contact surfaces has been approached by either geometrical contact models, which can be very complex (Hivet and Boisse, 2005), or simplified rules combined with FEM computations (Lomov et al., 2007), or deformation computations acting alone (Wang and Sun, 2001). The topology-based method for correcting interpenetrations proposed here is by contrast very simple and needs no deformation calculation. It is expressed in two widely applicable sorting algorithms, whose execution simultaneously, and without intervention, predicts the shapes of contact zones.

The approach proposed in this paper forms a complementary alternative to deformation modeling, being based entirely on empirical data for the final textile geometry and therefore needing no knowledge of the processing history of the textile or its constitutive properties.

The textile geometry is analyzed at the scale of fiber tows. The question of how fibers are distributed within a single tow is also important, but will be treated separately, because it requires a different probabilistic formulation.

The method is demonstrated on a 3D angle interlock composite of carbon fiber tows in a ceramic matrix (Fig. 2). The statistics of a large ensemble of virtual samples are compared to target statistics established by μCT data.

2. Preliminary notes on describing a textile architecture

2.1. Topology

Textile topology refers to the pattern of tow interlacing that defines a textile architecture. Topology will be described by a set of spatial orderings among pairs of tows. The orderings arise at the time the textile is fabricated on a weaving or braiding machine and are in one-to-one correspondence with the discrete actions of the textile machinery.

Consider, for example, the orderings of warp and weft tows in a woven fabric. The "warp tows" are a set of approximately parallel yarns that are held in tension during weaving. The "weft tows" are inserted approximately perpendicular to the warp tows by a rapier or flying shuttle device that passes over some warp tows and beneath others. By controlling which subgroup of warp tows are passed over or under (by mounting each subgroup in a separate "harness" which moves the subgroup up or down between passages of the rapier or shuttle), different textile architectures are made. The motions of the harnesses cause permanent orderings of warp and weft tows in the through-thickness direction. Tows are also ordered in the in-plane directions. Each harness consists of a comb-like series of "heddles" (wires), each of which contains a hole through which one warp tow is threaded, so that the warp tows are held in fixed order across the fabric. Weft tows are ordered along the warp axis by their order of insertion in time. Two textile architectures are distinct if and only if they possess different sets of tow orderings.

The following formulation of topological rules to describe such orderings is applicable to any textile, e.g., weave or braid, that consists of tows interlaced in such a way that no tow crosses another tow more than once. A common example

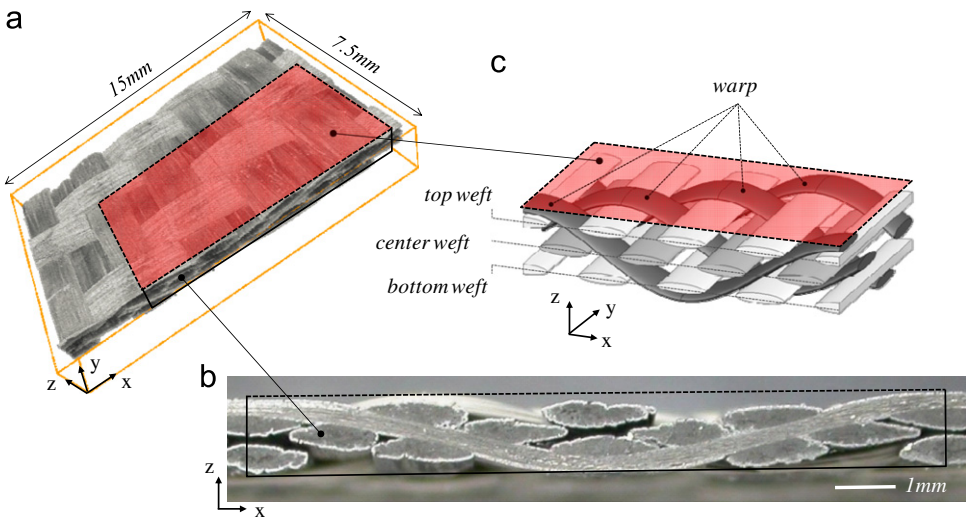

Fig. 2. The angle interlock architecture of the subject material: (a) 3D μCT image (Bale et al., 2011), (b) optical image of a cross-section along the warp direction shows that specimens have been rigidified by a ceramic matrix coating (white layer surrounding each tow), (c) idealized schematic of the unit cell, which extends one warp period along the *x*-axis and comprises four warp tows along the *y*-axis. Four tow genuses are identified: *warp*, *top weft*, *center weft*, and *bottom weft*.

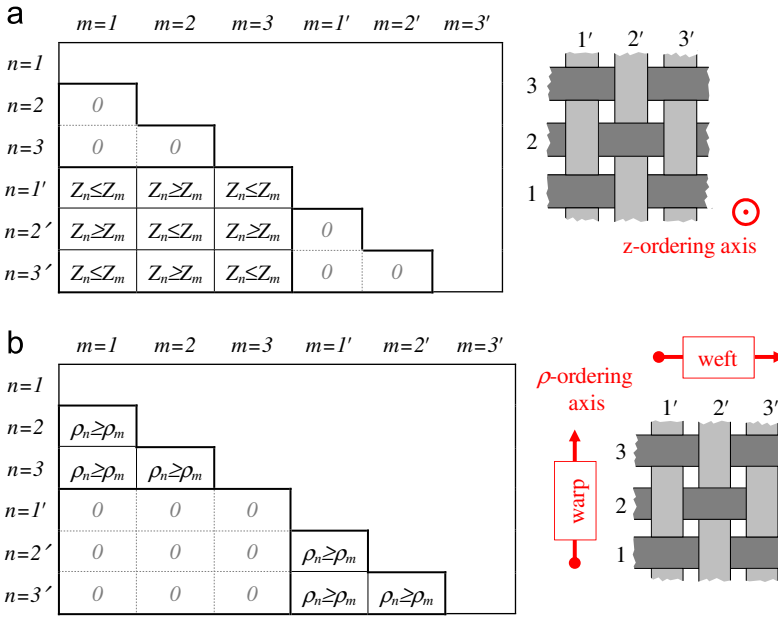

Fig. 3. (a) *z*-ordering matrix for the three warp and three weft tows in the inset figure, with warp tows numbered 1–3 and weft tows 1′–3′. (b) ρ-ordering matrix for the same segment of fabric. The axes to which orderings refer are shown in the inset figures.

of a textile that satisfies this condition is a plain weave. In a plain weave, pairs of warp and pairs of weft tows do not cross over each other, while each weft tow crosses each warp tow just once (Fig. 3). Other textiles satisfying the one-crossover restriction include textiles with non-orthogonal tows, such as a 2D triaxial braid, and 3D interlock weaves, one of which will be used below to exemplify the geometry generation algorithm. Multi-ply lay-ups of textiles in which each ply satisfies the one-crossover restriction will also usually satisfy the restriction and can therefore be addressed with minor modification to the book-keeping of topological rules. However, certain more complex textile patterns, e.g., some 3D braids and knits, do not satisfy the restriction and would require a significantly different approach.

It is useful to classify the tows in a textile into "genuses," a new term we introduce, defined in such a way that tows within a single genus are equivalent to one another in the repeating structure of the textile. Warp and weft tows are always assigned different genuses; but two warp tows (or two weft tows) may or may not belong to the same genus, depending on the details of the weave type. For example, in a plain weave textile, the warp tows are assigned to one genus ("warp genus") and the weft to a second ("weft genus") and only two genuses need be identified (Fig. 3). But in the

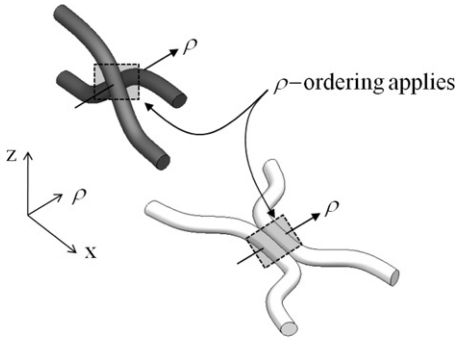

Fig. 4. In-plane ordering (or ρ-ordering) applies where the projections of two tows on a plane perpendicular to the ρ-axis overlap. Two possible cases illustrated are a "crossing" configuration (top) and a "kissing" configuration (bottom).

exemplar angle interlock weave, three genuses of weft tow are defined (Fig. 2(c)). The reasons why two weft tows might be assigned to different genuses in this architecture are explained below.

Let a finite specimen of a generic textile contain N_g genuses, each containing n_k tows ($k=1,\ldots,N_g$). Let $N_t=\sum_k n_k$ denote the total number of tows in the textile. For textiles satisfying the one-crossover restriction, the orderings that define the textile topology are specified for pairs of tows as follows.

(a) ***z-ordering***

Orderings in the z-direction (through-thickness) are specified as an array, $O^{(z)}$, of logical expressions, with the entry for any pair of tows m and n taking one of three possible values:

$$O^{(z)}_{mn}=\begin{cases} Z_m \geq Z_n & \text{if } \Omega_m \neq \Omega_n \text{ and } m \text{ above } n \\ Z_m \leq Z_n & \text{if } \Omega_m \neq \Omega_n \text{ and } m \text{ below } n \\ \text{indeterminate} & \text{if } \Omega_m = \Omega_n \end{cases} \qquad (m=1,\ldots,N_t;\ \ n=1,\ldots,N_t) \tag{1}$$

where Ω_m is the genus to which tow m belongs, Z_m represents the interval along the z-axis occupied by tow m, and "above" or "below" means shifted towards positive or negative z, respectively. The condition $Z_m \geq Z_n$ or $Z_m \leq Z_n$ is enforced only at the cross-over between tow m and tow n; it does not require that tow m occupies higher or lower values of z everywhere than are occupied by tow n everywhere. The condition "indeterminate" means that any ordering of tows m and n is possible at any location. Where tows of the same genus do overlap (e.g., the parallel edges of warp tows), their ordering might be determined indirectly if a tow of a different genus is also present (e.g., a weft tow), since they might both be ordered with respect to the third tow at that location; but, if no third tow intervenes, any ordering can occur.

Orderings can only be specified between pairs of tows. It is generally not possible to establish a single ranking of all tows. In particular, the fact that $Z_m > Z_n$ and $Z_n \geq Z_p$ does not imply that $Z_m \geq Z_p$ (textiles would not hold together if it did!).

For a plain weave, the elements of the z-ordering array are as shown in Fig. 3(a).

(b) ***in-plane ordering*** **(ρ-ordering)**

Orderings in the in-plane directions (x–y plane) are specified as a second array of logical expressions, $O^{(\rho)}$, with the entry for any pair of tows i and j taking one of three possible values:

$$O^{(\rho)}_{mn}=\begin{cases} \rho_m \geq \rho_n & \text{if } \Omega_m = \Omega_n \text{ and } m \text{ right of } n \\ \rho_m \leq \rho_n & \text{if } \Omega_m = \Omega_n \text{ and } m \text{ left of } n \\ \text{indeterminate} & \text{if } \Omega_m \neq \Omega_n \end{cases} \qquad (m=1,\ldots,N_t;\ \ n=1,\ldots,N_t) \tag{2}$$

where the ρ-axis (either the x or y-axis) lies normal to the dominant in-plane direction of the axes of tows of a given genus, ρ_m represents an interval occupied along the ρ-axis by tow m, and "right of" or "left of" means shifted towards higher or lower values of ρ, respectively. Examples of ρ-axes are shown in Fig. 3(b). The condition $\rho_m \geq \rho_n$ or $\rho_m \leq \rho_n$ is enforced only where the projections of two tows on a plane normal to the ρ-axis cross over one another; it does not require that tow m occupies higher or lower values of ρ everywhere than are occupied by tow n everywhere. Two possible configurations where ρ-ordering might be violated, the "crossing" and "kissing" configurations, are shown in Fig. 4. For a plain weave, the elements of the ρ-ordering array are as shown in Fig. 3(b).

Looking at the regular and simple example of Fig. 3, it may appear that sorting tows into their correct order is an exercise in the obvious, for which the formality of the ordering arrays is superfluous. However, when considering patches of different tows that interpenetrate within a small volume of a highly deformed, irregular textile, finding an algorithm that relieves interpenetration correctly can be challenging. Incorrect re-orderings applied locally lead to a cascade of incorrect conditions elsewhere, which are not obviously resolved. The ordering arrays make the choice of correction

straightforward. They have the empowering quality that their use makes the same, simple algorithms for sorting interpenetrations applicable to *any* textile architecture that satisfies the single-crossover restriction, without modification. The topology of any textile can be defined by its ordering arrays $O^{(z)}$ and $O^{(\rho)}$.

2.2. Geometry

The geometry of a textile reinforcement is defined by the shape of individual tows, including local variations and long-range variations due to global deformation. Following the image analysis developed by Bale et al. (2011), tow geometry is described in terms of the sections of the tow perpendicular to its nominal axis, which is usually chosen to be an axis in a global Cartesian system. For each tow m, the coordinates of the centroid of its section, $(\xi,z)^{(m)}$ ($\xi \equiv y$ for warp tows and $\xi \equiv x$ for weft tows), along with its area, $A^{(m)}$, aspect ratio, $ar^{(m)}$, and orientation, $\theta^{(m)}$ (rotation about the tow axis), are specified as continuously varying functions of position along the tow. Only components of the centroid position that are orthogonal to the nominal direction of a tow need to be generated, the other component being a deterministic point (independent variable) on a computational grid, which is introduced below. Thus, five random variables $\{\xi^{(m)},z^{(m)},A^{(m)},ar^{(m)},\theta^{(m)}\}$ describe the geometry of tow m at each of a sequence of sections.

The objective of the present work is to generate tow shapes whose statistics match experimental data. The pertinent statistics are those of the variables in the set $\{\xi^{(m)},z^{(m)},A^{(m)},ar^{(m)},\theta^{(m)}\}$.

3. Computational procedure

3.1. Experimental data

For nominally periodic textiles, the experimental data for each variable in the set $\{\xi^{(m)},z^{(m)},A^{(m)},ar^{(m)},\theta^{(m)}\}$ can be decomposed into non-stochastic, periodic variations and non-periodic, stochastic variations (Bale et al., 2011):

$$(\xi,z)_i^{(m)} = \left\langle (\xi,z)_i^{(m)} \right\rangle + (\delta\xi,\delta z)^{(m)} \tag{3a}$$

$$A_i^{(m)} = \left\langle A_i^{(m)} \right\rangle + \delta A^{(m)} \tag{3b}$$

$$ar_i^{(m)} = \left\langle ar_i^{(m)} \right\rangle + \delta ar^{(m)} \tag{3c}$$

$$\theta_i^{(m)} = \left\langle \theta_i^{(m)} \right\rangle + \delta\theta^{(m)} \tag{3d}$$

where $\langle \ldots \rangle$ indicates an average value and subscript i refers to a grid point along the reference period. The first term on the right hand side in Eq. (3) is the non-stochastic, periodic variation of the variable and the second term is the deviation of the variable from its average. The deviations are assumed statistically independent of the grid point.

The average terms and the deviations in Eq. (3) are deduced from experimental data by translating data for nominally equivalent points throughout a specimen onto one of N_ϕ discrete grid points lying within a "reference" period for each tow genus, a process called "reference period collation." The reference period is a single cycle of the periodic variations of tows of that genus in the textile and the nominally equivalent points are those related to a point on the reference period by translation through a lattice vector of the periodic structure (see Bale et al. (2011) for details). The translated data are collated and their average spatial variation and root-mean-square deviation (RMSD) from this average value determined.

Other statistics computed from data include the "correlation length" for each variable, which specifies how far two points on a tow must be separated for the deviations of the variable at those points to be approximately independent of one another. Correlations are also determined between the deviations of different variables on the same tow. Analysis of the data for the particular material studied by Bale et al. (2011) revealed negligible or weak correlations between any two variables within a single tow, which are therefore not explicitly introduced in the following. Thus, the set of experimental data that will be considered in the formulation is:

$$\begin{aligned}
&D = \{D_k, k = 1,\ldots,N_g\}\\
&D_k = D_k^{(av)} \cup \{\sigma_\xi^{(k)},\sigma_z^{(k)},\sigma_A^{(k)},\sigma_{ar}^{(k)},\sigma_\theta^{(k)},\zeta_\xi^{(k)},\zeta_z^{(k)},\zeta_A^{(k)},\zeta_{ar}^{(k)},\zeta_\theta^{(k)}\}\\
&D_k^{(av)} = \left\{ \left\langle \xi_i^{(k)} \right\rangle, \left\langle z_i^{(k)} \right\rangle, \left\langle A_i^{(k)} \right\rangle, \left\langle ar_i^{(k)} \right\rangle, \left\langle \theta_i^{(k)} \right\rangle,\ i = 1,\ldots,N_\phi \right\}\\
&\quad (\xi \equiv y \text{ for warp tows and } \xi \equiv x \text{ for weft tows})
\end{aligned} \tag{4}$$

where D_k contains the data for tow genus k; σ denotes the RMSD of a variable (e.g., σ_ξ or σ_z refer to the deviations $\delta\xi$ or δz, respectively); ζ denotes the correlation length for the deviations of a variable along a tow (e.g., ζ_ξ or ζ_z refer to the deviations $\delta\xi$ or δz, respectively); and the quantities in parentheses $\langle \ldots \rangle$ refer to the averaged quantities of Eq. (3), which express non-stochastic periodic variations as functions of position along a tow.

In addition to Eq. (4), experimental data are analyzed to determine correlation parameters that measure how strongly the deviations of variables on one tow influence those on another tow at tow crossovers. For the data presented by Bale

et al. (2011), significant inter-tow correlations are found only for the deviations δz. A minor amendment of the method to deal with this correlation was described in Blacklock et al. (2012).

3.2. Generation of trial tow shapes

Using Monte Carlo methods, replica specimens of the textile are generated from the experimental statistics. The procedure consists of three main steps: generating trial tow positions and shapes using a Markov Chain generator (Blacklock et al., 2012); correcting any errors (interpenetration of tows or improper tow ordering) by applying correction algorithms based on topological ordering rules; and smoothing away small unphysical irregularities. If necessary, the procedure is iterated using minor adjustments of the input data to ensure that target statistics are reproduced.

The Markov Chain generator creates replicas of each tow in a textile sample, one tow at a time, working directly from the experimental data set, D. The sample to be produced can contain any number of tows of any specified length, so that the virtual specimen can be much larger than the real specimen from which the experimental data were derived. The trial geometry of tow m is generated on a discrete grid as follows.

A sequence of values of each of the five variables $\{\xi^{(m)},z^{(m)},A^{(m)},ar^{(m)},\theta^{(m)}\}$ is created along the desired length of tow m, proceeding one variable at a time. Treating variables one at a time, rather than simultaneously, is valid if correlations between different variables at any point on the same tow are small. This condition is satisfied for the data analyzed in Bale et al. (2011). For each variable, z for example, the non-stochastic, periodic variation is generated by concatenating sufficiently many repetitions of the average quantity $\{\langle z_i^{(k)}\rangle, i=1,\ldots,N_\phi\}$, computed directly from data for the tow genus, k, to which tow m belongs. Next, a Markov Chain operator, i.e., a "Probability Transition Matrix" (PTM), is calibrated by the datum RMSD and correlation length for that variable and genus, e.g., $\sigma_z^{(k)}$ and $\zeta_z^{(k)}$, following the methods described in Blacklock et al. (2012). The calibrated PTM is then applied to generate a sequence of values of the deviation of the variable at successive grid points along the tow, spanning its whole length. These steps are repeated for each variable. The outcome of these steps is a sequence of values of the parameter set $\{\xi^{(m)},z^{(m)},A^{(m)},ar^{(m)},\theta^{(m)}\}$, which are used to define elliptical trial tow cross-sections at each grid point along the axis of the tow. Thus, after the first step in the generation procedure, each tow takes the form of a stochastic, irregular elliptical cylinder represented by its sections on a discrete grid.

The use of ellipses in these preliminary steps is a reasonable but not necessary choice, and does not require that the experimental or final generated sections are close to elliptical. First, fitting ellipses is only one convenient method of extracting cross-sectional geometrical parameters from experimental data; other methods are also possible for determining the five section characteristics (center of mass, area, aspect ratio, and orientation) from data, including methods based on the calculation of first and second moments of the mass distribution in which no trial shape need be assumed. Second, while tow sections are introduced into the 3D generator as ellipses, they could equally be introduced as rectangles or other shapes; and they do not remain elliptical as the generation steps proceed.

Tow generation is completed by discretizing each section (Fig. 5). This is done by representing every tow, of all genuses, on a common rectangular grid $\{(X_i,Y_j), i=1,\ldots, N_x, j=1,\ldots, N_y\}$ defined on the x–y plane, i.e., the plane of the textile sheet. Thus in a weave with warp tows aligned nominally along the x-axis, tow m, a warp tow, for example, is defined by a set of sections on successive grid rows i, each of which is a set of coordinate pairs:

$$T^{(m)} = \{T_i^{(m)}, i = 1,\ldots,N_x\}$$
$$T_i^{(m)} = \{(z_<^{(m)}(i,j), z_>^{(m)}(i,j)), j = j_<^{(m)}(i),\ldots,j_>^{(m)}(i)\} \quad \text{(warp tow)} \tag{5}$$

where $z_<^{(m)}(i,j)$ and $z_>^{(m)}(i,j)$ define the lower and upper surfaces of the tow at grid point (i,j); and $j_<^{(m)}(i)$ and $j_>^{(m)}(i)$ are the minimum and maximum values of the grid index j occupied by the tow on its section on grid row i (Fig. 5). An analogous definition applies for a weft tow (perpendicular to the warps), with row i and column j interchanged.

3.3. Removal of errors – enforcement of topological orderings

The generation steps described above are repeated to create all tows. During this process, the generated tows are offset from one another to comply with the measured average tow separation and the relative phases implied by the definition of

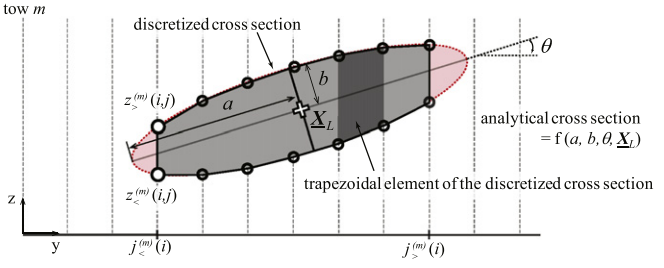

Fig. 5. A section of tow m on a grid plane perpendicular to the tow axis. On the discrete grid, an initially elliptical section is represented by a concatenation of quadrilaterals. Further departures from the elliptical outline arise during the removal of ordering errors between tows.

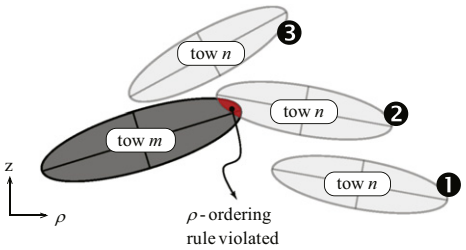

Fig. 6. Three hypothetical positions for the section of tow n relative to the section of tow m on the same grid plane, for two tows of the same genus. In discussions in the text, the ordering $\rho_m < \rho_n$ is assumed.

the textile (see the treatment of the tow axis variables, $\{x,y,z\}^{(m)}$, in Blacklock et al. (2012)). Because the non-stochastic periodic variations in the generated tows are based on data and tend to be larger than the stochastic deviations, the resulting textile replica tends to be consistent with the experimentally measured textile. In particular, tows tend to move up, down, and sideways just as necessary to avoid one another as they interlace. However, some significant errors (physically disallowed features) can be present, because each tow follows the trajectory dictated by its own generation algorithm, without detailed checking to see where it lies relative to other tows. Thus, instances of tows interpenetrating or parts of tows being out of sequence can occur and are in fact common. Such instances are violations of the topological rules of the textile. The next step in the process of generating a replica is therefore to systematically remove all instances of topological error. This is accomplished by enforcing the ordering rules of Eqs. (1) and (2) via a pair of correction algorithms, one for the in-plane or ρ-ordering rules, $O^{(\rho)}$, and another for the z-ordering rules, $O^{(z)}$. Applying the correction algorithms is simplified by the rectangular discretization of the problem.

(a) ***notation for ordering***

Suppose tows m and n occupy the intervals $Z_m = [z_<^{(m)}(i,j), z_>^{(m)}(i,j)]$ and $Z_n = [z_<^{(n)}(i,j), z_>^{(n)}(i,j)]$ at a grid point (i,j), which they both inhabit. When comparing the ordering of the two tows in the z-direction, three ordering states are distinguished:

$$\begin{aligned} &Z_m > Z_n \quad \text{if } z_<^{(m)}(i,j) \geq z_>^{(n)}(i,j) \\ &Z_m < Z_n \quad \text{if } z_>^{(m)}(i,j) \leq z_>^{(n)}(i,j) \\ &Z_m \text{ and } Z_n \text{ overlap otherwise} \end{aligned} \tag{6}$$

In regard to the third state, different possible cases of overlap need not be distinguished when applying the ordering algorithms. Eq. (6) may be referenced for pairs of tows having the same or different genus.

(b) ***enforcing ρ-ordering – the "edge retreat" algorithm***

The sections of two tows of the same genus on a grid plane commonly exhibit a few typical cases of relative position (Fig. 6). Assume that the ordering rule for tows m and n is that $\rho_m < \rho_n$. Of the three illustrated positions for tow n, positions 1 and 3 satisfy the ordering rule, while position 2 violates it, because it involves interpenetration. Position 3 does not violate ρ-ordering, because, even though the intervals ρ_m and ρ_n along the ρ-axis overlap, the overlap occurs where the projections of the two tows on the z-axis are separated. Thus the tows overhang one another, a common and topologically admissible variation for tows of the same genus.

The following correction algorithm accepts all non-interpenetrating variations as satisfying ρ-ordering, with the exception of instances of overhang that neighbor instances of interpenetration, as specified below.

Take any pair of tows m and n of the same genus. Consider the example of two warp tows, aligned nominally with the x-axis. First, a scan is performed along the x-direction, searching for interpenetrations of the sections of the two tows. Interpenetration is flagged when the intervals $[z_<^{(m)}(i,j), z_>^{(m)}(i,j)]$ and $[z_<^{(n)}(i,j), z_>^{(n)}(i,j)]$ occupied by the tows in the z-direction at grid point (i,j) overlap. A typical case of interpenetration on the i^{th} row of the grid is shown in Fig. 7(a).

The edge retreat algorithm consists of eliminating pairs of points on each of the two tows on grid row i until the limit points $j_>^{(m)}(i)$ and $j_<^{(n)}(i)$ are equal and the residual tow sections obey the ordering $\rho_m \leq \rho_n$. The grid point j that will be the new location of $j_>^{(m)}(i)$ and $j_<^{(n)}(i)$ is chosen as the average of their old values, shifted to the next higher integer value if necessary. Shifting consistently in one direction minimizes roughness in the resulting tow geometry.

The edge retreat step applied to row i leaves a single common grid point for the two tows on that grid row, which is tagged as a common point or "tow abutment." There is no need for the intervals occupied by two tows in the z-direction to be the same at the abutment (Fig. 7(b)).

The fact that the plane of abutment left by the edge retreat step is always parallel to the z-axis is consistent with the fact that interpenetration between tows of the same genus tends to occur in one of the two cross-over configurations

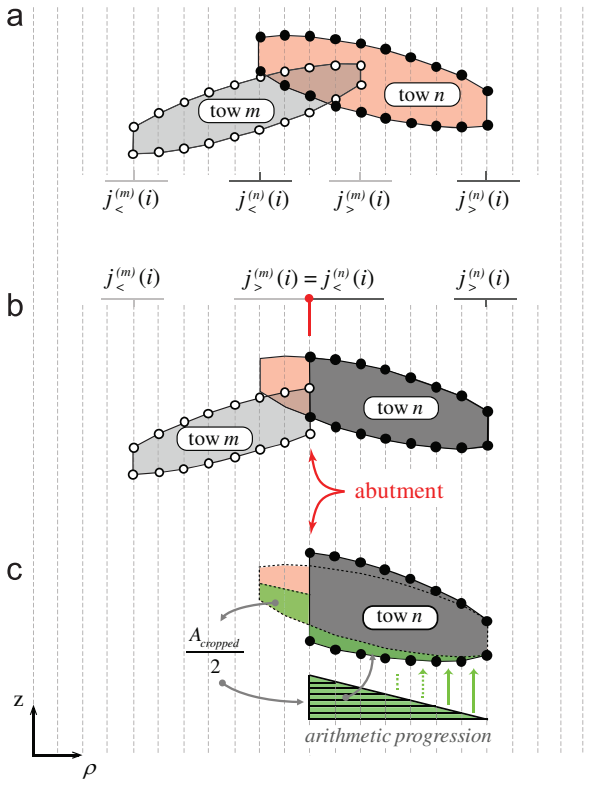

Fig. 7. The edge retreat algorithm applied to two tows of the same genus, with the ordering requirement $\rho_m > \rho_n$. (a) configuration before edge retreat, (b) configuration after edge retreat. The remaining common gridpoint is tagged as an abutment between the two tows. (c) re-shaped tows after linearly-varying dilation to preserve the cross-sectional area. Compare the flat contact facets created by edge retreat with the datum images in Fig. 8.

sketched in Fig. 4. Tows pressed into contact along their edges tend to form flat contact surfaces approximately parallel to the z-axis. However, distortion of the shape of the abutment surface that results from the edge retreat algorithm is still possible when the tow shapes are modified after the correct textile topology is established (see below).

For every pair of tows m and n of the same genus, the edge retreat correction is applied one row at a time to all the rows that satisfy either of the following conditions:

(i) The intervals $[z_<^{(m)}(i,j), z_>^{(m)}(i,j)]$ and $[z_<^{(n)}(i,j), z_>^{(n)}(i,j)]$ overlap for any j on row i.

(ii) Tows m and n share common grid points on row i and the ordering of the intervals $[z_<^{(m)}(i,j), z_>^{(m)}(i,j)]$ and $[z_<^{(n)}(i,j), z_>^{(n)}(i,j)]$ at any point j on row i differs from the ordering of the intervals $[z_<^{(m)}(i\pm1,j'), z_>^{(m)}(i\pm1,j')]$ and $[z_<^{(n)}(i\pm1,j'), z_>^{(n)}(i\pm1,j')]$ at any point j' on either row $i-1$ or row $i+1$, where a difference in ordering is determined by considering the three states defined in Eq. (6).

Application of (b) means that two tows of the same genus can share common grid points (overhang one another) only where there is a gap between the tows in the z-direction over the interval of the overhang and for the rows on either side of the interval of the overhang. This rule ensures that no interpenetration of tows occurs when the sections of tows are later joined into solid bodies.

(c) *z-ordering algorithm*

Interpenetration between tows of different genus is removed by applying the following z-ordering algorithm to one grid point (i,j) at a time.

At any multiply occupied grid point, there exists a set of intervals $[z_<^{(m_1)}(i,j), z_>^{(m_1)}(i,j)]$, $[z_<^{(m_2)}(i,j), z_>^{(m_2)}(i,j)]$, $[z_<^{(m_3)}(i,j), z_>^{(m_3)}(i,j)]$,…, occupied by the set of tows $S_{ij}=\{m_1, m_2, m_3, \ldots\}$. The number of tows inhabiting the grid point might be anything from zero to ~10 in a typical engineering textile, depending on the architecture (Ko 1989). The required z-ordering of these tows is specified by the ordering array $O^{(z)}$. The z-ordering algorithm consists of moving the intervals $[z_<^{(m_1)}(i,j), z_>^{(m_1)}(i,j)]$, $[z_<^{(m_2)}(i,j), z_>^{(m_2)}(i,j)]$, etc., at the single grid point (i,j) in the z-direction to ensure that the known orderings of all pairs of tows inhabiting the grid point are obeyed. The distinct orderings that need to be considered are those in Eq. (6).

The ordering rules in $O^{(z)}$ act on pairs of tows of different genus, the ordering of pairs of tows of the same genus being indeterminate. If all tows in the set S_{ij} are of different genuses, their pair-wise orderings imply a unique overall ordering on that grid point. (Instances of conflicting pair-wise orderings arising between tows in S_{ij} virtually never occur. They require cohabitation of a grid point by multiple, distinct pieces of the same tow, which can only occur if the tow possesses re-entrant features on its cross-section. Such re-entrant features are unexpected and never seen in the exemplary material).

For realistic input data, no more than two tows of any one genus are found in S_{ij}, but this case is relatively common, arising wherever edge overhang occurs (e.g., case 3 of Fig. 6). When two tows of one genus are included in S_{ij}, their relative ordering is indeterminate unless a tow of a different genus is present in S_{ij} and that tow is ordered above one of the pair and below the other.

Ordering errors can be corrected in the following steps:

(i) A pair-wise search over S_{ij} is performed to identify all tows involved in an ordering error. Those tows are then collected into subsets of S_{ij}, denoted $s_{ij}^{(p)}$, $p=1,\ldots$, and defined so that the tows within any subset exhibit ordering errors with one another but not with any tow that is not in that subset. This separation resolves the correction procedure into corrections dealing, for example, with tows near the top of a section and those near the bottom.

(ii) Ordering corrections are then performed within each subset, invoking $O^{(z)}$.
- If $s_{ij}^{(p)}$ contains no two tows of the same genus, the outcome of sorting $s_{ij}^{(p)}$ is unique.
- If $s_{ij}^{(p)}$ contains two tows of the same genus, there must necessarily also be at least one tow of a different genus present in $s_{ij}^{(p)}$ (otherwise there could be no ordering error). If one other such tow is ordered above one of the pair of the same genus and below the other, the outcome of sorting by invoking $O^{(z)}$ is unique. But if all tows of a different genus are ordered either above or below both the tows of the same genus, the ordering of the same-genus pair remains indeterminate. In such cases, their ordering relative to one another is left unchanged.

(iii) The outcome of step (ii) is a revised ordering of the tows in $s_{ij}^{(p)}$, stated as an ordered list of indexing integers. To complete the ordering correction, the tows must be assigned new intervals on z, $[z_<^{(m)}(i,j),z_>^{(m)}(i,j)]$, for all $m \in s_{ij}^{(p)}$, that are correctly ordered and in contact with one another (share a common z-interval boundary). The specification of the intervals is a question of geometry, addressed in the next section.

(iv) After new intervals are assigned, new overlap could possibly arise between two different subsets $s_{ij}^{(p)}$. These are eliminated with rapid convergence by making the two overlapping sets a single set and re-applying steps (i)–(iii).

3.4. Adjustments of geometry

Many plausible rules could be applied for adjusting tow geometry during z-ordering and edge-retreat corrections. The following emphasize preservation of the cross-sectional area of the tow. The cross-sectional area determines the local fiber packing density, which has a significant effect on local properties, and thus load distributions and failure mechanisms.

Changes in the aspect ratio and orientation of tow sections due to ordering error corrections are left uncontrolled, but usually modest. Furthermore, their role in failure mechanisms is expected to be secondary to that of the cross-sectional area.

(a) ***Adjustments of tow cross-sections after edge retreat***

During application of the edge retreat algorithm, changes can arise in the area and aspect ratio of tow cross-sections. To maintain the tow cross-sectional area, the tow is dilated in the z-direction. The dilation factor decreases linearly from a relatively large value at the edge of the tow that has retreated to unity at the far edge (Fig. 7(c)). The magnitude of the dilation factor is chosen to conserve the cross-sectional area of the tow.

(b) ***Adjustments of tow cross-sections after z-ordering***

Consider a subset $s_{ij}^{(p)}$ of n_p tows with mutual ordering errors. Following re-ordering, the intervals occupied by the tows along the z-axis, $\{[z_<^{(m)}(i,j),z_>^{(m)}(i,j)],m \in s_{ij}^{(p)}]\}$, are redefined so that:

(i) The intervals are contiguous, i.e., $z_>^{(m)}(i,j) = z_<^{(n)}(i,j)$ where m and n are successive intervals in the corrected ordering.

(ii) The length of each interval, $z_>^{(m)}(i,j)-z_<^{(m)}(i,j)$, is unchanged.

(iii) The center of mass of the intervals, $z^{(p)} = \sum(z_>^{(m)}(i,j)^2-z_>^{(m)}(i,j)^2)/2$, where the sum is made over $s_{ij}^{(p)}$, is unchanged.

After this adjustment, $s_{ij}^{(p)}$ consists effectively of a single interval of length $\sum z_>^{(m)}(i,j)-z_>^{(m)}(i,j)$ centered at $z^{(p)}$. All pairs of tows in $s_{ij}^{(p)}$ that are contiguous are tagged as contacting at grid point (i,j).

The above procedure has the advantage that the area of any section of a tow remains unchanged (because the intervals $[z_{<}^{(m)}(i,j),z_{>}^{(m)}(i,j)]$ defining the tow are held constant), while the change in the centroid of a tow section, averaged over all tow sections, is minimized (because the center of mass of all the tows inhabiting any grid point, measured along the z-direction, is held constant).

(c) ***Smoothing of non-physical irregularities***

Three sources of physically unrealistic irregularities in tow boundaries are present in the specimen generator algorithm. The first is the Markov chain operator, which can introduce mesh-dependent, small wavelength oscillations in the deviation of any of the stochastic variables $\{\xi^{(m)},z^{(m)},A^{(m)},ar^{(m)},\theta^{(m)}\}$. The second is the use of a discrete grid in the $\{x,y\}$ plane, which introduces steps in the lateral boundaries of tows (the boundaries seen in projections onto the $\{x,y\}$ plane). The latter irregularities can be exacerbated by the use of the edge retreat algorithm to correct ρ-ordering errors. The third is the process of correcting z-ordering errors, which can leave gradients in the z-coordinate of tows at the edge of a region of interpenetration that are larger than could be followed by the fibers in the tow.

All these types of irregularity have spatial wavelengths that are approximately commensurate with the mesh size chosen in the discretization of the problem. The mesh size should be much less than the width of tows and therefore much less than all correlation lengths, which tend to be approximately equal to or greater than the tow width (or the distance between cross-overs). Therefore, the irregularities can be removed without impairing the fidelity of the generator by applying a smoothing operation, in which stochastic variables are averaged over a moving box with a gage length less than the tow width. A modified moving box averaging algorithm that tends to conserve the RMSD of the deviations was presented in Blacklock et al. (2012).

Smoothing of irregularities created by the Markov chain operator can be removed by a single smoothing operation immediately following the generation of stochastic tow variables, before solid tows are discretized or ordering corrections are applied. Smoothing of irregularities caused by the discrete grid (Appendix A) requires the introduction of x and y coordinates for points on the edge of a tow that do not lie on the grid. Such smoothing must be done after all other steps in tow generation are complete. To ensure that no new interpenetration is introduced, new points on the tow edge must lie within the existing volume of the tow.

Smoothing of irregularities due to z-ordering corrections is achieved by the modified moving box average algorithm. The smoothing is applied only along the nominal fiber direction and not in the transverse tow direction. Smoothness along the fiber direction is implied by fiber continuity; on the other hand, irregularities on tow boundaries in the transverse direction are accommodated by fiber-fiber shear and are observed in real specimens (e.g., Fig. 2(c)) and should therefore be left in the model.

3.5. Possible necessity of iteration

The ordering corrections, smoothing steps, and adjustments of tow section shape can in principle alter the statistics of the tows. If the target statistics were used as input, they may not be matched by those of the generated virtual specimens. If the discrepancies are significant, an iterative procedure would be required, modifying the input statistics until the output statistics hit the targets. However, at least for the exemplary textile of this paper, this proves unnecessary (see below).

3.6. Creation of 3D tow models

Once a physically valid model has been achieved by manipulating tow cross-sections, solid tow representations are finished by joining tow sections with flat facets, filling the space between successive sections with eight-noded or six-noded polyhedra. Connectivity between the polyhedra is then provided by shared nodes. Such solid elements are the final output for transfer into finite element codes.

4. Illustration for a 3D angle interlock weave.

4.1. Subject material and data from μCT images

The material used as an example is illustrated in Fig. 2. It consists of T300 carbon fiber tows woven in an angle interlock architecture and rigidified by a coating of SiC deposited by chemical vapor infiltration. Details of the material and its imaging and statistical analysis can be found in Bale et al. (2011). The subject weave contains a single genus of warp tows and three genuses of weft tows, labeled top weft, center weft, and bottom weft (Fig. 2(c)). The unit cell contains four warp tows, each with period λ_x in the warp direction and separated by a nominal interval $\lambda_y/4$ in the weft direction (Fig. 2(c)). Successive warp tows (tows with increasing x coordinate) are shifted by $\lambda_x/4$ along the warp direction. In a unit cell, four tows are present within each weft genus and have a period λ_y in the weft direction. Successive weft tows in any genus (tows with increasing y coordinate) are separated by $\lambda_x/4$ in the warp direction and shifted by $-\lambda_y/4$ in the weft direction.

The architecture of the angle interlock is defined by the orderings $O^{(z)}$ and $O^{(\rho)}$, which are displayed for a single unit cell in Tables 1 and 2. In a specimen of arbitrary size, $O^{(z)}$ and $O^{(\rho)}$ must be defined for every pair of tows present.

Table 1
z-ordering in the exemplary angle-interlock weave (Fig. 2(c)). The z-ordering matrix is exhibited for a single unit cell sample, comprising four warps and 12 weft tows (four per genus), numbered as depicted in the schematic. The inset figure also shows the z-ordering axis. Only one half of the matrix needs to be filled. Six regions are identified representing the pairings of the four genuses. With m the column index and n the row index, "$\leq$" means $Z_m \leq Z_n$ while "$\geq$"means $Z_m \geq Z_n$. Entry "0" is shorthand for "indeterminate" z-ordering.

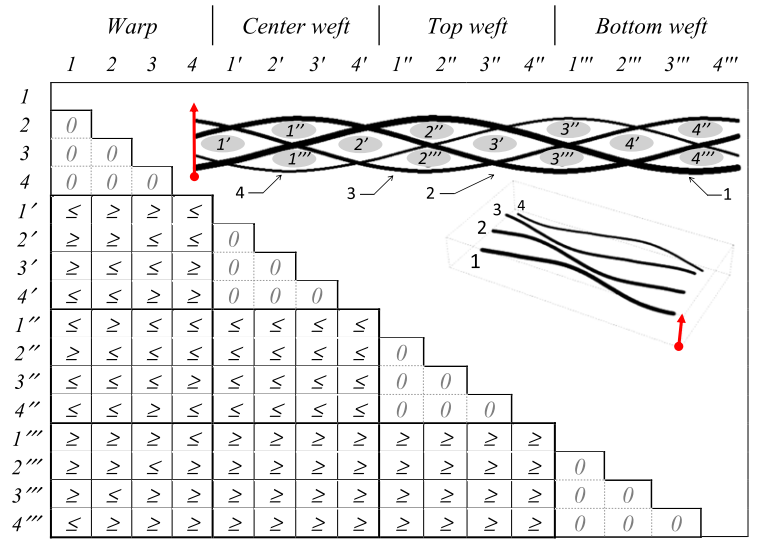

Table 2
ρ-ordering in the exemplary angle-interlock weave (Fig. 2(c)). The ρ-ordering matrix is exhibited for a single unit cell sample, comprising four warps and 12 weft tows (four per genus), numbered as depicted in the schematic. The inset figure also shows the ρ-ordering axis for weft (dashed arrow) and warp (continuous arrow) tows. Only one half of the matrix needs to be filled. Four regions are identified representing the pairings within each of the four genuses. With m the column index and n the row index, "$\leq$" means $\rho_m \leq \rho_n$. Entry "0" is shorthand for "indeterminate" ρ-ordering.

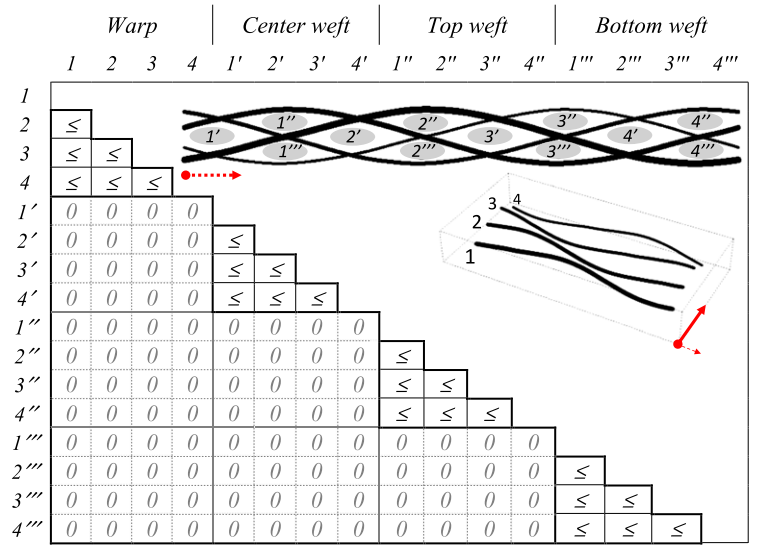

The complete set of input data required for the geometry generator, i.e., the data set of Eq. (4), was established by analyzing μCT images. Reference period collation was used to partition the data into non-stochastic, periodic contributions (or systematic contributions) and stochastic, non-periodic contributions (Bale et al., 2011).

A typical cross-section of a warp tow in the subject material is presented in Fig. 8. In this example, the ellipses fitted for data analysis for warp tows 2 and 3 overlap. Such instances in the datum images suggest that overlap is likely to arise in generated stochastic tows with the same variability in locus and shape parameters. Furthermore, where the two tows in the experimental image abut, their surfaces possess flat vertical facets, similar to those introduced by the edge retreat

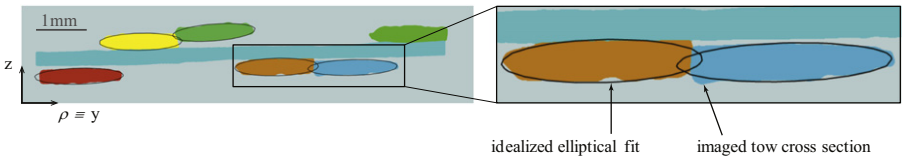

Fig. 8. Ellipses fitted to cross-sections of warp tows in a 2D image slice from a μCT experiment.

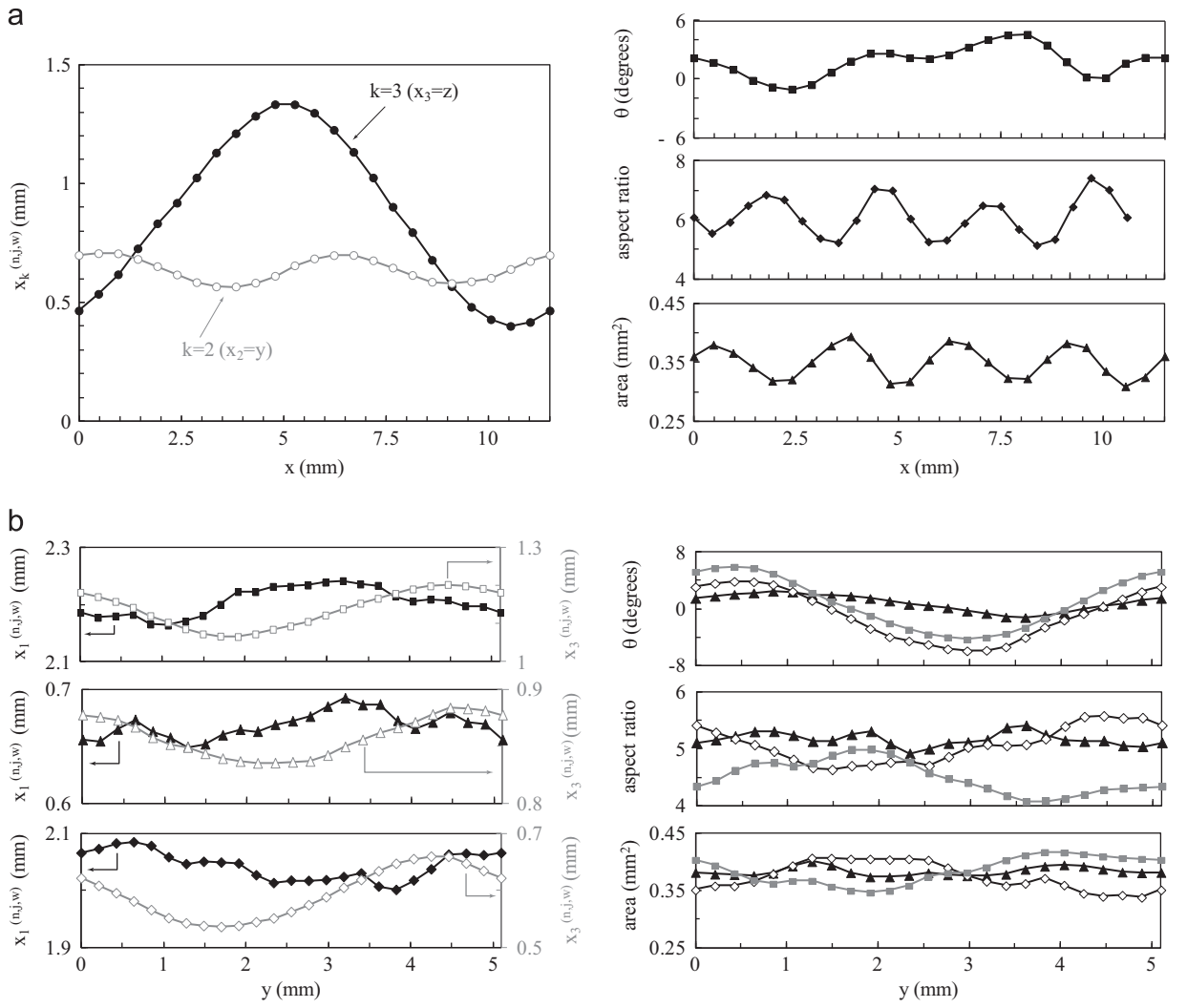

Fig. 9. Experimental data: the non-stochastic, periodic variations of all five variables used to characterize tows, plotted along the nominal direction of the tow axis (figures reorganized from Bale et al., 2011): (a) warp genus: profiles along *x*-axis, (b) the three wefts genuses (square: top wefts/triangle: center wefts/diamond: bottom wefts): profiles along the *y*-axis.

procedure (Fig. 7).[1] Thus the edge retreat procedure is true to the shape deformation that occurs in reality when two tows are pressed into one another edgewise.

The systematic variations, $D^{(k)}$, of all five variables are shown in Fig. 9 for each tow genus, k. The standard deviations, $\sigma^{(k)}$, and the correlation length, $\zeta^{(k)}$, for all parameters appear in Table 3.

The objective of the virtual specimen generator is to match the measured statistics from experimental data. Thus, the data of Fig. 9 and Table 3 are the target statistics for the generator and must be reproduced in large ensembles of virtual specimens.

[1] The same flat vertical contact feature can also be observed in Fig. 2 of Badel et al. (2008).

Table 3
Values of stochastic parameters for the four genuses identified in the 3D-interlock fabric.

x (locus)		y (locus)		z (locus)		Area		Aspect ratio		Angle	
$\sigma^{(\delta x,i)}$ (mm)	$\zeta^{(\delta x,i)}$ (mm)	$\sigma^{(\delta y,i)}$ (mm)	$\zeta^{(\delta y,i)}$ (mm)	$\sigma^{(\delta z,i)}$ ((mm^2)	$\zeta^{(\delta z,i)}$ (mm)	$\sigma^{(A,i)}$ (mm^2)	$\zeta^{(A,i)}$ (mm)	$\sigma^{(ar,i)}$ (mm)	$\zeta^{(ar,i)}$ (mm)	$\sigma^{(\theta,i)}$ deg.	$\zeta^{(\theta,i)}$ (mm)
Warp tows ($i=w$)											
–	–	0.021	3.5	0.034	3.65	0.017	3.4	0.787	10.6	0.89	4.2
Top weft tows ($i=tw$)											
0.068	3.4	–	–	0.029	5.3	0.010	3.1	0.302	20.3	0.775	7.9
Center weft tows ($i=cw$)											
0.077	3.9	–	–	0.016	5.9	0.015	3.4	0.706	16.7	0.925	16.6
Bottom weft tows ($i=bw$)											
0.071	4.0	–	–	0.024	4.5	0.015	3.8	0.337	6.3	0.939	13.1

4.2. Generation steps

Virtual specimens are generated by the Monte Carlo method, using the *Mathematica 7.0* software package (Wolfram Research, Inc, 2010). Random values of variables are assigned using a numerical pseudo-random number generator.

(a) ***Tow generation***

A practical first choice is to use the experimental statistics, which are also the target statistics, as the input for the generator (i.e., to calibrate the Markov Chain algorithm, as detailed in Blacklock et al. (2012)), in the expectation that the generator will not significantly shift the statistics of a large ensemble of virtual specimens as it manipulates individual cases.

The initial parametric representation of an individual tow is created in three steps, which are repeated for each of the stochastic variables in turn.

First, non-stochastic, periodic variations of one of the variables are generated by concatenating copies of the systematic data for a single reference period, e.g., $\{\langle \xi_i^{(k)} \rangle, i=1,\ldots,N_\varphi\}$, to form a tow of a prescribed length, as described above. If the grid used to discretize the 3D problem in $\{x,y\}$ space has different mesh size from that used to specify $\{\langle \xi_i^{(k)} \rangle, i=1,\ldots,N_\varphi\}$ for the reference period, linear interpolation is used to map from one to the other.

Second, the Markov Chain algorithm of Blacklock et al. (2012) is used to generate sequences of non-periodic, stochastic deviations in the variable at successive grid points along the tow axis. To eliminate grid effects arising from the Markov Chain operator, the stochastic deviation can be smoothed to remove mesh-dependent small-scale fluctuations, using the modified moving box average described by Blacklock et al. (2012) (box of width ± 1, four recursions). The usefulness of performing a smoothing operation at this stage of the 3D tow generation procedure is examined below.

Third, the non-stochastic, periodic and stochastic, non-periodic contributions are summed.

The above steps applied to the tow loci variables $\{\xi^{(m)},z^{(m)}\}$ generate 1D stochastic tow loci of the type described in Blacklock et al. (2012). With the generalization introduced in this paper, they also create values of the complete set of variables $\{\xi^{(m)},z^{(m)},A^{(m)},ar^{(m)},\theta^{(m)}\}$ for successive grid planes $x=x_i$ or $y=y_i$ (for warp or weft tows) occupied by any tow. In the generalized case, the variable set is used to form an elliptical section for the tow on each grid plane, which is converted to a sequence of pairs of z coordinates at each grid point occupied by the section (Fig. 5). When discretized, the cross-section becomes a concatenation of trapezoids, whose vertices are manipulated in subsequent generation steps.

(b) ***Ordering corrections and shape adjustment***

A sequence of seven generation steps combining the removal of interpenetrations, adjustment of sectional shapes to preserve area, and smoothing were used to form the final model in this example. The sequence is detailed in Fig. 10.

Defining separate top, center, and bottom genuses for the weft tows, has one significant effect on the ordering operations. Because ρ-ordering is only applied to tows of the same genus, the kissing configuration of Fig. 3 never appears as a ρ-ordering violation for weft tows; weft tows of the same genus are always well separated along the x-axis (warp direction) in the exemplar material. Instances of two weft tows interpenetrating in the kissing configuration involve tows of different genus and are therefore are resolved by the z-ordering correction.

(c) ***Variations during processing steps***

The tow loci and shape characteristics undergo minor fluctuations when the model is discretized and during ordering corrections, which can be minimized by mesh refinement and well-chosen numerical methods (Appendix A). For the procedures used in the calculations reported in this paper, the fluctuations in area are small compared to the variations associated with the periodicity of the textile. The most important measures of fidelity are the statistics of an ensemble of specimens, which are analyzed below.

(d) ***Combining tows with matrix***

The virtual specimen is defined in this paper as the set of tows only. The real specimens for which the calibrating data were taken possessed very little matrix, consisting of a thin layer of ceramic deposited on the surfaces of tows (Fig. 2(b)).

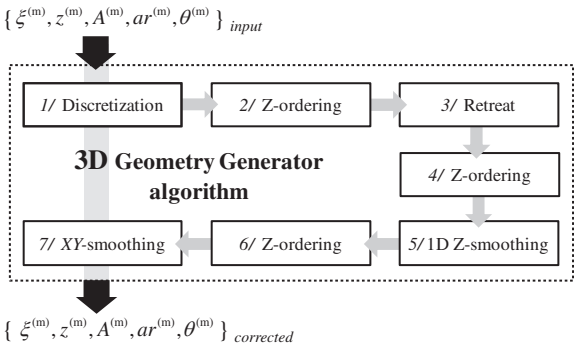

Fig. 10. Steps used within 3D generator for exemplar weave. Both the input and output (corrected) can be characterized by the five stochastic cross-sectional shape variables.

If matrix were added in real specimens to fill out a larger volume, e.g., filling the composite out to upper and lower molding platens, matrix domains can be readily added in the virtual specimens as spatial complements of the tow domains.

4.3. *Illustration with only loci treated as stochastic variables*

In the first illustration of the method, only the tow loci variables $\{\xi^{(m)},z^{(m)}\}$ are treated as stochastic, the shape variables $\{A^{(m)},ar^{(m)},\theta^{(m)}\}$ being treated as deterministic (deviations with zero RMSD). Reducing the set of stochastic variables allows a simpler examination of the effects of random initial tow positions on the performance of the generator formulation.

A representative virtual specimen created by the generation steps defined above is shown in Fig. 11. The grid spacing chosen both for specimen generation and the statistical analysis of an ensemble of specimens was approximately 0.1 mm, with $N_x=120$ (warp direction) and $N_y=60$ (weft direction). The grid spacing is approximately 5–10% of the tow width. Mesh dependent shape aberrations in the final geometry are commensurate with the grid spacing, but can be further reduced in a post-processing step as described in Section 3.4(c).

Tow geometry statistics – virtual* vs. *real

To test whether the generated virtual specimens possess the target statistics, i.e., the statistics supplied from experiment, a statistical analysis was performed of an ensemble of 200 generated tow models. Each member of the ensemble consisted of a single unit cell of the textile architecture, comprising 4 warp and 12 weft tows.

The statistical analysis exactly mimicked the analysis of the original μCT data. Systematic variations were determined by the method of reference period collation, as described in Bale et al., 2011. Deviations were defined relative to these systematic curves and the RMSD and correlation length for the deviations were determined. Thus a complete set of output statistics was compiled, in one-to-one correspondence with the input data of Eq. (4).

The input and output systematic deviations are compared for warp tows in Fig. 12 (see Appendix B for similar results for weft tows). The systematic curves are essentially independent of the specimen size and the ensemble size for ensembles as large as that considered. Three cases are shown, differing in how the three steps used to implement the Markov chain algorithm were executed:

(i) "Markov": deviations generated by the Markov Chain operator without correlations between warp and weft tows and without smoothing;
(ii) "Smoothed": deviations generated by the Markov Chain operator without correlations between warp and weft tows and then smoothed using the moving box average; and
(iii) "Cross-correlated": deviations generated by the Markov Chain operator with correlations between warp and weft tow z-deviations at cross-over locations.

The systematic curves are shown for the experimental data, after the generation of 1D initial tow loci, and after the generation of the final 3D tow geometry. The systematic curves for the tow loci coordinates show negligible shift throughout the generation procedure. The curves for the tow area show a small shift in the final 3D model output, which is a mesh density effect with contributions also from ordering and smoothing operations. Overall, the non-stochastic systematic curves remain acceptably close to the experimental curves, which are the target curves for the generator. Thus the targets are achieved.

The statistics of deviations are listed in Table 4. The RMSDs for the deviations in tow loci coordinates show no statistically significant differences for any of the three cases (a)–(c). Furthermore, they are all within expected variance of the experimental target RMSDs. The correlation lengths for deviations vary somewhat more, but without forming clear trends. The variability of correlation lengths reflects the sensitivity of the fitting procedure used to evaluate a correlation length to the details of a particular specimen (see Appendix A of Blacklock et al. (2012)).

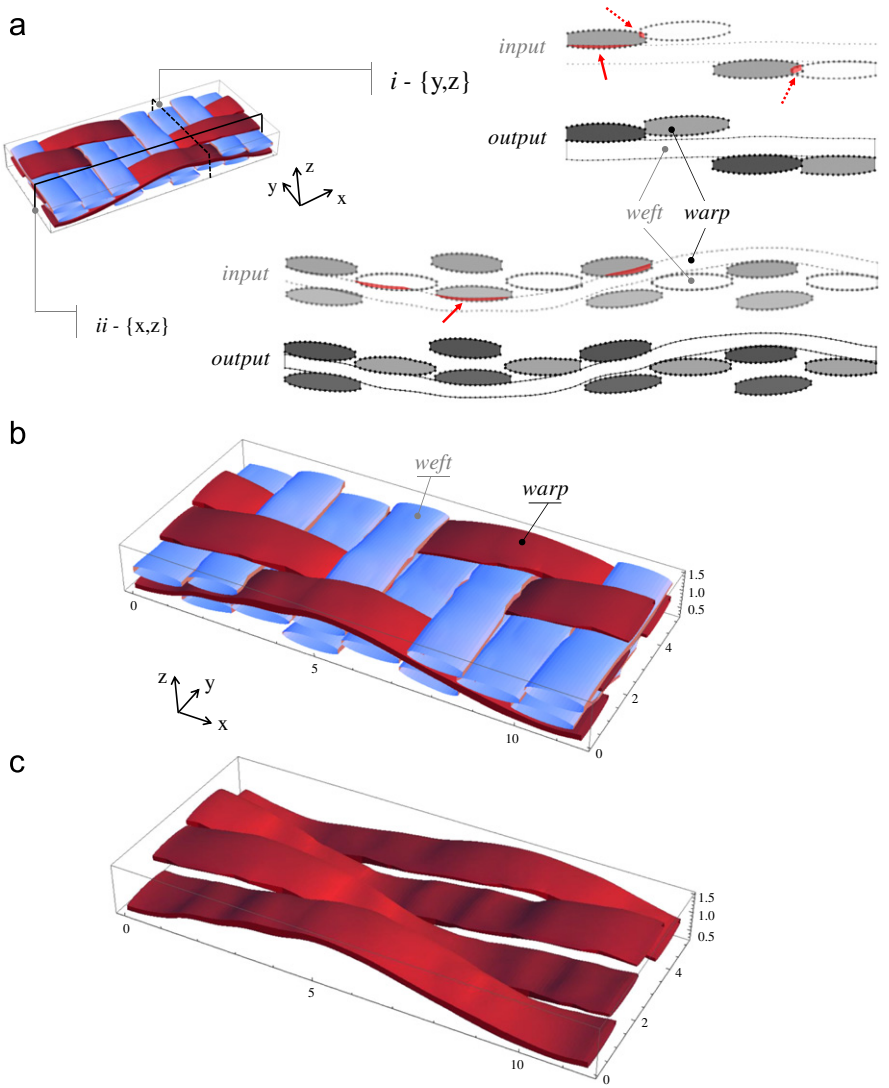

Fig. 11. Virtual specimen one unit cell in size, defined on a grid with $N_x=120$ and $N_y=60$. (a) Illustration of interpenetration removal on two different cross sections perpendicular to the warp (i) and weft (ii) tows, respectively. Both input and output geometries are displayed. Continuous and dashed arrows locate region where interpenetration occurs, violating z-ordering and ρ-ordering rules, respectively. Repair exploits (i) edge retreat and (ii) z-ordering following the topological rule: $Z_m \geq Z_n$. (b) 3D rendering of the output corrected virtual specimen. (c) 3D rendering of the output warp tows only.

The comparison of the three cases (a)–(c) shows that there is no advantage (or disadvantage) in applying smoothing to the generated 1D tow loci if they are to be used as input in the 3D tow generator. The smoothing operations in the 3D tow generation cover the same purpose.

In a further statistical study, the RMSDs for each stochastic variable were computed separately for each virtual specimen in the generated ensemble and histograms of the RMSD values were compiled (Fig. 13). The width of the distribution of RMSD values about the mean varies approximately as $W^{-1/2}$, where W is the specimen size. As Fig. 13 shows, variations in the RMSD from specimen to specimen are substantial when the specimen size is comparable to the unit cell.

In summary, the statistical analysis of the generated ensemble shows that the target statistics have been achieved satisfactorily when the experimental statistics were used as input for the generation procedure.

5. Discussion

For textile composites possessing nominal periodicity, the approach of reference period collation followed in this paper, in which all variables are resolved into non-stochastic, periodic variations and stochastic, non-periodic deviations, enables efficient use of often limited experimental data. However, periodicity is not always present, even nominally. But even in

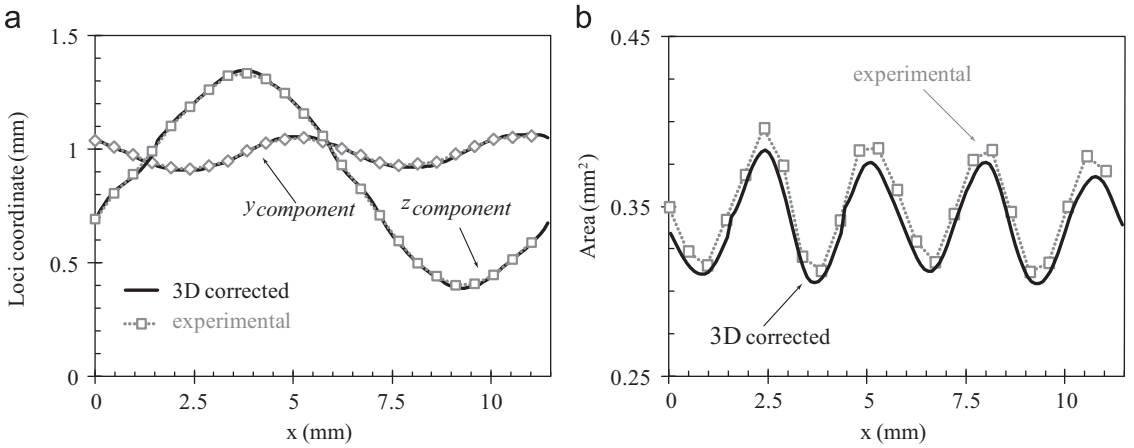

Fig. 12. Comparison of experimental and output systematic curves for warp tows when using the procedure called "Markov" (see text), with grid $N_x=120$, $N_y=60$. (a) y and z coordinates of the tow locus. (b) cross-sectional area.

Table 4
Statistics computed for ensemble of generated virtual specimens.

Procedure[a]	x (locus)		y (locus)		z (locus)	
	$\sigma^{(\delta x,i)}$ (mm)	$\zeta^{(\delta x,i)}$ (mm)	$\sigma^{(\delta y,i)}$ (mm)	$\zeta^{(\delta y,i)}$ (mm)	$\sigma^{(\delta z,i)}$ (mm)	$\zeta^{(\delta z,i)}$ (mm)
Warp tows ($i=w$)						
Exp.	_	_	*0.021*	*3.5*	*0.034*	*3.65*
Mark.	_	_	0.0198	6.797	0.0264	6.801
Sm.	_	_	0.0193	9.116	0.0257	9.117
X-cor.	_	_	0.0197	6.787	0.0276	5.141
Top weft tows ($i=tw$)						
Exp.	*0.068*	*3.4*	_	_	*0.029*	*5.3*
Mark.	0.0606	6.669	_	_	0.0237	7.619
Sm.	0.0606	7.986	_	_	0.0237	8.423
X-cor.	0.0606	6.669	_	_	0.0254	9.741
Center weft tows ($i=cw$)						
Exp.	*0.077*	*3.9*	_	_	*0.016*	*5.9*
Mark.	0.0656	7.347	_	_	0.0144	8.255
Sm.	0.0657	8.808	_	_	0.0143	8.987
X-cor.	0.0656	7.347	_	_	0.0164	10.084
Bottom weft tows ($i=bw$)						
Exp.	*0.071*	*4.0*	_	_	*0.024*	*4.5*
Mark.	0.0676	8.074	_	_	0.0194	6.686
Sm.	0.0680	9.424	_	_	0.0195	7.675
X-cor.	0.0676	8.074	_	_	0.021	7.890

[a] Exp.=experimental (the target statistics); Mark.="Markov"; Sm.="smoothed"; X-cor.="cross correlated" (see text for full explanations of procedures).

such general cases, key aspects of the formulation remain appropriate. In particular, the application of topological rules for resolving interpenetrations and ordering errors via the edge retreat and z-ordering corrections, and the computationally convenient mapping of the problem onto a fixed grid in the $\{x,y\}$ plane, remain viable.

Part of the generation process is based on the Markov chain algorithm introduced by Blacklock et al. (2012). For the Markov chain algorithm to be a valid method, correlations between stochastic variables on different tows must generally be small. While Blacklock et al. (2012) showed an effective adaptation to treat a single non-negligible inter-tow correlation, in the most general case, multiple non-negligible inter-tow correlations can be envisaged. Such cases will require non-Markovian models. The remarks made above for non-periodic textiles apply in such cases too: once the first tow representations have been generated by a non-Markovian model, the topological rules and rectangular $\{x,y\}$ discretization remain a viable approach to achieving physically permissible (interpenetration-free) virtual specimens.

This paper defers consideration of how the geometric models that have been generated can be conveniently ported into finite element codes and how physically reasonable models can be formulated within such codes to deal with the singular fields implied by the presence of contiguous strongly anisotropic tow domains. One plausible approach in such modeling

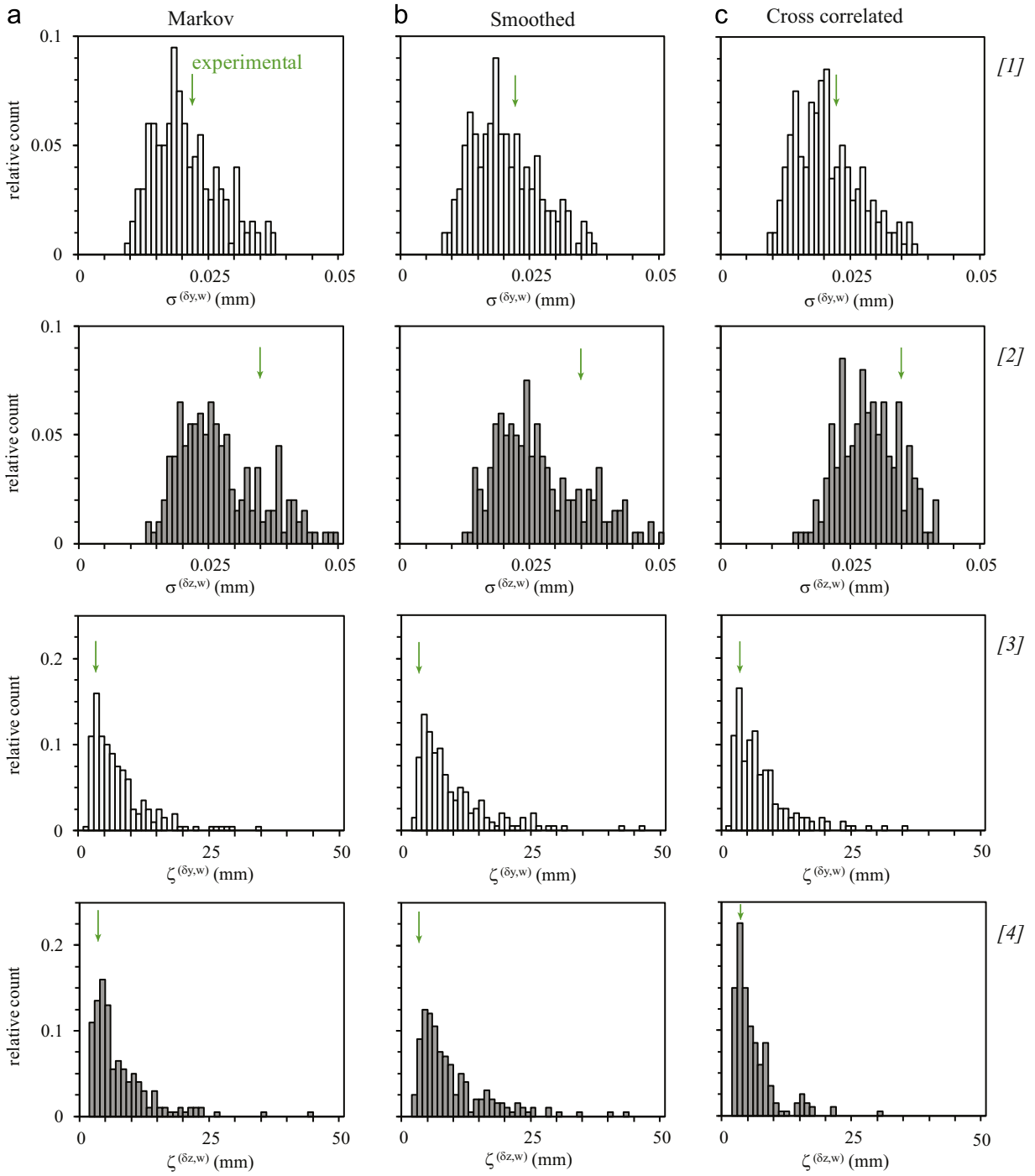

Fig. 13. Histograms of the statistics of deviations in an ensemble of 200 virtual specimens of size equal to the unit cell. Statistics are reported for the warp genus for the three different procedures defined in the text: (a) "Markov", (b) "smoothed", and (c) "cross-correlated". [1] RMSD of the deviation δy. [2] RMSD of the deviation δz. [3] RMSD of the deviation δA. [4] Correlation length for δy. [5] Correlation length for δz.

is to base predictions of local failure events within a textile body on gage-averaged stress or strain quantities, rather than quantities evaluated at points in space. Gage-averaging has the dual virtue that it greatly reduces or eliminates the singular fields associated with sharp tow features, while simultaneously representing non-linear fracture processes in a physically realistic manner (Yang and Cox, 2003). Controlling the effects of sharp tow features may be desirable because such features are in many cases aberrations of the tow representation rather than physically realistic (e.g., the sharp edges introduced in tow cross-sections by the discretization of Fig. 5). Supporting non-linear fracture models, such as cohesive models, is desirable because of their superiority to linear elastic fracture mechanics in all but the most brittle materials.

Encouraging results based on gage-averaging methods for predicting textile failure have recently been demonstrated for triaxial braids (Yang and Cox, 2010).

By adjusting the grid density, the formulation presented above allows considerable range in the degree of detail kept in the shapes of individual tows. Furthermore, once a valid, non-interpenetrating geometry has been established for each tow in a specimen, either grid refinement or grid coarsening is possible before the final output. One appealing limit to consider is the coarsest grid that could convey important tow characteristics into a finite element calculation. For tows of aspect ratio approximately 10, as in the carbon/SiC exemplar, a tow cross-section requires at least two elements to avoid numerical difficulties in finite element stress-strain computations. But even with only two elements, i.e., a tow cross-section consisting of just two trapezoids, most tow characteristics can still be incorporated in a virtual specimen: sufficient degrees of freedom are present to control the area, aspect ratio, orientation, and locus of the tow axis. In conjunction with gage-averaging approaches to the physics of failure, such coarse 3D tow representations might enable tractable models of textile composite components measuring tens of cm.

6. Concluding remarks

A computationally efficient method has been demonstrated for generating large ensembles of virtual textile specimens.

The method uses experimental data to establish non-stochastic, periodic variations and stochastic, non-periodic deviations in geometrical parameters. The experimental data used for illustration were acquired using μCT imaging, but could also be obtained by other means such as rapid serial sectioning. The final virtual specimens, with non-physical interpenetrations removed, are generated without invoking any model of fiber bundle or preform deformation, but rely only on the experimental data. Thus the method is complementary to methods based on simulating the mechanics of textile processing.

The statistical characteristics of an exemplary carbon fiber, SiC matrix composite were successfully reproduced.

Acknowledgments

This work was supported by the Air Force Office of Scientific Research (Dr. Ali Sayir) and NASA (Dr. Anthony Calomino) under the National Hypersonic Science Center for Materials and Structures (AFOSR Contract No. FA9550-09-1-0477). We acknowledge the use of data from the x-ray synchrotron micro-tomography beam line (8.3.2) at the Advanced Light Source (ALS) at the Lawrence Berkeley National Laboratory, which is supported by the Office of Science of the U.S. Department of Energy under contract No. DE AC02 05CH11231.

Appendix A. Minimization of grid effects

The tow loci and shape characteristics undergo minor fluctuations when the model is discretized and during ordering corrections. Fig. A.1 shows representative changes in the cross-sectional area of one particular tow in one virtual specimen: while the variation of the area with position along the tow is unaffected by the generation procedures, the area shifts consistently to slightly reduced values. The loss of area occurs mainly during discretization and is associated with the truncation of the elliptical trial shape at the last grid points occupied by the ellipse (Fig. 5). The same loss of area shows up in ensemble averages in the systematic curves for area (Figs. 12 and B.1). The steps of ordering correction, which are accompanied by area-conserving shape adjustments, do not shift the cross-sectional area (Fig. A.1).

This effect of discretization can be avoided by modifying the way elliptical trial cross-sections are discretized (Fig. 5), by (1) extending the cross-section to the next grid point whenever the extremum of the ellipse is closer to that point than

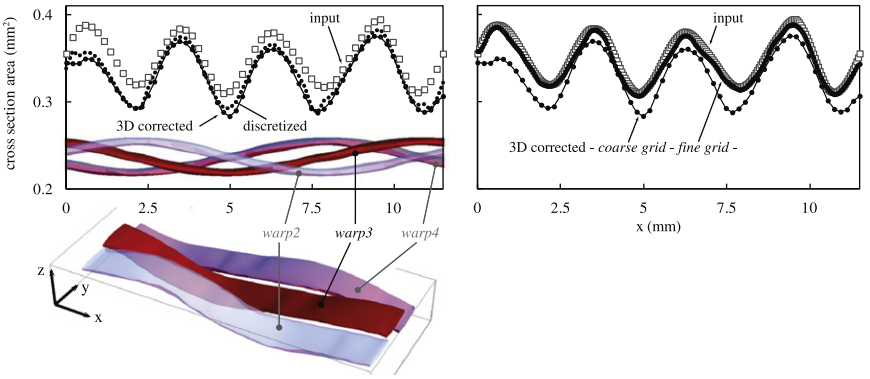

Fig. A.1. Effect of grid size on the area of one warp tow ("warp3") in one stochastic specimen at different stages of the 3D virtual specimen creation. (a) Coarse grid: $N_x=60$ and $N_y=30$. (b) Fine grid: $N_x=240$ and $N_y=120$. Comparison with the 3D image shows where edge retreat has acted on warp3: edge retreat followed by shape adjustment has caused no appreciable net effect on the tow.

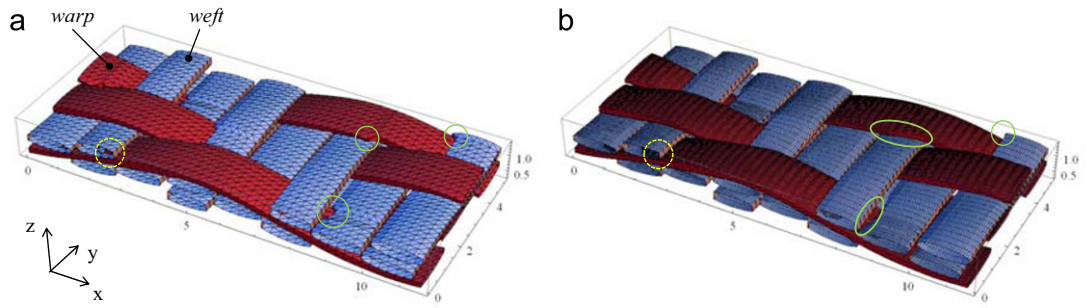

Fig. A.2. Virtual specimen one unit cell in size. (a) Coarse grid (N_x=50, N_y=25): solid circles highlight steps caused by the grid discretization; dashed circle locates a region where interpenetration is observed. (b) The magnitude of steps can be diminished by grid refinement. In this illustration, different refinements have been applied to warp and weft tows: for warp tows, N_x=50 and N_y=100, while for weft tows, N_x=200 and N_y=25. (Inconsistent grids are not preferred for other generation steps.) (a) Input and (b) Output.

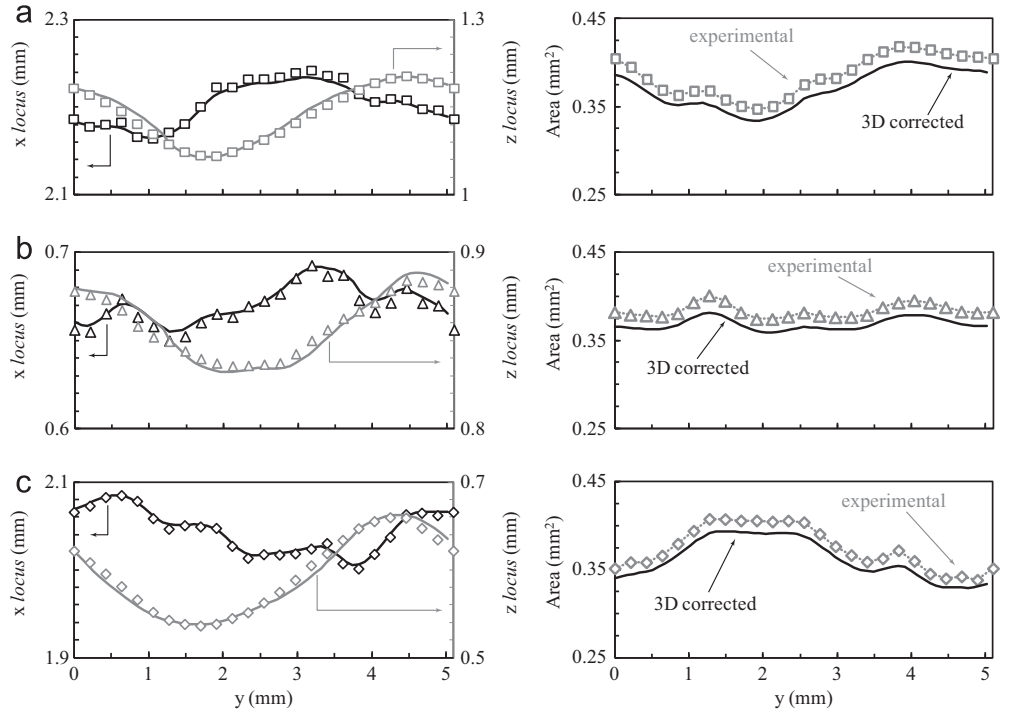

Fig. B.1. Comparison of experimental and output systematic curves for all 3 weft genuses when using the procedure called "Markov" (see text), with grid N_x=120, N_y=60. (a) top weft tows. (b) center weft tows. (c) bottom weft tows. *left figures*: *x and z coordinates of the tow locus – right figures*: *cross-sectional area.*

the last point occupied by the ellipse (i.e., sometimes rounding up the number of occupied grid points rather than always rounding down) and (2) modifying the assigned z values of the top and bottom surfaces of the tow section to ensure that area is conserved. The use of the first modification rather than just the second ensures minimization of changes in the aspect ratio.

A second effect of discretization is the introduction of steps in the edges of tows (Fig. A.2). These can be minimized by grid refinement, but this reduces the size of specimens that can be dealt with computationally. A preferred method is to remove the steps in a post-processing procedure, by introducing new points on tow surfaces that lie between grid points and allow smooth paths for tow surfaces ("*step 7*" in Fig. 10). This can be done without creating new ordering errors by constraining the new points to lie within the volumes bounded by the unmodified tow surfaces.

Appendix B. Systematic curves for weft tows in virtual specimen ensemble

The systematic curves for tow loci and cross-sectional areas of weft tows in a generated ensemble of 200 virtual specimens (as detailed in Section 4.3) are shown in Fig. B.1. The degree of agreement with target curves is similar to that found for warp tows. The generation procedure preserves the non-stochastic, periodic variations very well.

References

Badel, P., Vidal-Salle, E., Maire, E., Boisse, P., 2008. Simulation and tomography analysis of textile composite reinforcement deformation at the mesoscopic scale. Compos. Sci. Technol. 68, 2433–2440.

Bale, H., Blacklock, M., Begley, M.R., Ritchie, R.O., Marshall, D.B., Cox, B.N., 2011. Characterizing three-dimensional textile ceramic composites using synchrotron x-ray micro-computed-tomography. J. Am. Ceram. Soc. 95 (1), 392–402.

Blacklock, M., Bale, H., Begley, M.R., Cox, B.N., 2012. Generating virtual textile composite specimens using statistical data from micro-computed tomography: 1D tow representations for the Binary Model. J. Mech. Phys. Solids 60, 451–470.

Cox, B.N., 1989. Inductions from Monte Carlo simulations of small fatigue cracks. Eng. Fract. Mech. 33, 655–670.

Cox, B.N., Carter, W.C., Fleck, N.A., 1994. A Binary Model of textile composites: I formulation. Acta Metall. Mater. 42, 3463–3479.

Cox, B.N., Yang, Q.D., 2006. In quest of virtual tests for structural composites. Science 314, 1102–1107.

Doob, J.L., 1953. Stochastic Processes. John Wiley and Sons, New York.

Grinstead, C.M., Snell, J.L., 1997. Introduction to Probability. American Mathematical Society.

Grishanov, S., Meshkov, V., Omelchenko, A., 2009a. A topological study of textile structures: Part I: an introduction to topological methods. Text. Res. J. 79 (8), 702–713.

Grishanov, S., Meshkov, V., Omelchenko, A., 2009b. A topological study of textile structures: Part II: topological invariants in application to textile structures. Text. Res. J. 79 (9), 822–836.

Groeber, M., Ghosh, S., Uchic, M.D., Dimiduk, D.M., 2008. A framework for automated analysis and simulation of 3D polycrystalline microstructures. Part 2: synthetic structure generation. Acta Mater. 56, 1274–1287.

Hivet, G., Boisse, P., 2005. Consistent 3D geometrical model of fabric elementary cell. Application to a meshing preprocessor for 3D finite element analysis. Finite Elem. Anal. Des. 42, 25–49.

Hivet, G., Boisse, P., 2008. Consistent mesoscopic mechanical behaviour model for woven composite reinforcements in biaxial tension. Composites Part B 39 (2), 345–361.

Howard, R., Markov, A.A., 1971. Extension of the Limit Theorems of Probability Theory to a Sum of Variables Connected in a Chain. Markov Chains, Appendix B, Vol. 1. John Wiley and Sons, New York.

Jiao, Y., Stillinger, F.H., Torquato, S., 2009. A superior descriptor of random textures and its predictive capacity. PNAS 106 (42), 17634–17639.

Ko, F.K., 1989. Preform fiber architecture for ceramic-matrix composites. Ceram. Bull. 68 (2), 401–414.

Lomov, S.V., Ivanov, D.S., Verpoest, I., Zako, M., Kurashiki, T., Nakai, H., Hirosawa, S., 2007. Meso-FE modelling of textile composites: road map, data flow and algorithms. Compos. Sci. Technol. 67, 1870–1891.

Lomov, S.V., Perie, G., Ivanov, D.S., Verpoest, I., Marsal, D., 2011. Modeling three-dimensional fabrics and three-dimensional reinforced composites: challenges and solutions. Text. Res. J. 81 (1), 28–41.

Lomov, S.V. and Verpoest I. (2002). Modelling of the internal structure and deformability of textile reinforcements: WiseTex Software. 10th European Conf. Composite Materials (ECCM-10).

Marshall, D.B., Cox, B.N., 2008. Integral textile ceramic structures. Annu. Rev. Mater. Res. 38, 425–443.

Miao, Y., Zhou, E., Wang, Y.Q., Cheeseman, B.A., 2008. Mechanics of textile mechanics: micro-geometry. Compos. Sci. Technol., 1671–1678.

Miyazaki, T., Shimajiri, M., Yamada, H., Seki, Itoh, H., 1995. A knitting pattern recognition and stitch symbol generating system for knit designing. Comput. Ind. Eng. 29, 669–673.

Pastore, C.M., Bogdanovich, A.E., Gowayed, Y.A., 1993. Applications of a meso-volume-based analysis for textile composite structures. Compos. Eng. 3 (2), 181–194.

Pollock, T.M., Allison, J.E., Backman, D.G., Boyce, M.C., Gersh, M., Holm, E.A., LeSar, R., Long, M., Powell Jr., A.C., Schirra, J.J., Whitis, D.D., Woodward, C., 2008. Integrated computational materials engineering: A Transformational Discipline for Improved Competitiveness and National Security. National Research Council of the National Academies, Washington, D.C..

Rugg, K.L., Cox, B.N., 2004. Deformation mechanisms of dry textile preforms under mixed compressive and shear loading. J. Reinf. Plast. Compos. 23 (13), 1425–1442.

Sullivan, B. and Yurus D. (2010). Generation and calibration of 3D woven preform design code for ceramic matrix composite materials. 34th Annual Conference on Composites, Materials, and Structures.

Terpant, G., Krishnaswami, P., Wang, Y., 2002. Computational prediction of yarn structure of 3-D braided composites. ASTM STP 1416, composite materials: Testing, Design, and Acceptance Criteria. In: Zereick, A., Nettles, A.T. (Eds.), , American Society for Testing and Materials International.

Wang, Y., Sun, X., 2001. Digital element simulation of textile process. J. Compos. Sci. Technol.

Wolfram Research Inc., 2010. Mathematica. Version 7.0, Champaign, IL.

Xiao, M., Geng, Z., 2010. A model of rigid bodies for plain-weave fabrics. Text. Res. J. 80 (19), 1995–2006.

Xu, J., Cox, B.N., McGlockton, M.A., Carter, W.C., 1995. A Binary Model of textile composites: II: elastic regime. Acta Metall. Mater. 43, 3511–3524.

Yang, Q.D., Cox, B.N., 2003. Spatially averaged local strains in textile composites via the Binary Model formulation. J. Eng. Mater. Technol. 125, 418–425.

Yang, Q.D., Cox, B.N., 2010. Predicting failure in textile composites using the Binary Model with gage averaging. Eng. Fract. Mech. 77, 3174–3189.